LETTER

Widely tunable broadband deep-ultraviolet to visible wavelength generation by the cross phase modulation in a hollow-core photonic crystal fiber cladding

To cite this article: J H Yuan *et al* 2013 *Laser Phys. Lett.* **10** 085402

IOP Publishing Laser Physics Letters
Laser Phys. Lett. **10** (2013) 085402 (5pp) doi:10.1088/1612-2011/10/8/085402

LETTER

Widely tunable broadband deep-ultraviolet to visible wavelength generation by the cross phase modulation in a hollow-core photonic crystal fiber cladding

J H Yuan[1,2], X Z Sang[1], Q Wu[1,3], C X Yu[1], G Y Zhou[2,4], X W Shen[1], K R Wang[1], B B Yan[1], Y L Teng[1], C M Xia[2], Y Han[4], S G Li[4], G Farrell[1,3] and L T Hou[4]

[1] State Key Laboratory of Information Photonics and Optical Communications, Beijing University of Posts and Telecommunications, PO Box 163 (BUPT), 100876 Beijing, People's Republic of China
[2] Laboratory of Nanophotonic Functional Materials and Devices, South China Normal University, 510006 Guangzhou, People's Republic of China
[3] Photonics Research Center, School of Electronic and Communications Engineering, Dublin Institute of Technology, Kevin Street, Dublin 8, Ireland
[4] Institute of Infrared Optical Fibers and Sensors, Physics Department, Yanshan University, 066004 Qinhuangdao, People's Republic of China

E-mail: yuanjinhui81@163.com

Received 13 June 2012, in final form 2 April 2013
Accepted for publication 8 April 2013
Published 2 July 2013
Online at stacks.iop.org/LPL/10/085402

Abstract
The deep-ultraviolet (UV) to visible wavelengths are efficiently generated for the first time by the cross phase modulation (XPM) between the red-shifted solitons and the blue-shifted dispersive waves (DWs) in the fundamental guided mode of the multi-knots of a hollow-core photonic crystal fiber cladding (HC-PCFC). When the femtosecond pulses with a wavelength of 850 nm and average power of 300 mW are coupled into the knots 1–3, the conversion efficiency η_{uv-v} of 11% and bandwidth B_{uv-v} of 100 nm in the deep-UV region are experimentally obtained. The multi-milliwatt ultrashort pulses are tunable over the deep-UV (below 200 nm) to visible spectral region by adjusting the wavelengths of the pump pulses in different knots. It is expected that these widely tunable broadband ultrashort deep-UV–visible pulse sources could have important applications in ultrafast photonics, femtochemisty, photobiology, and UV–visible resonant Raman scattering.

(Some figures may appear in colour only in the online journal)

1. Introduction

Photonic crystal fibers (PCFs) open up new horizons in nonlinear optics due to their unique dispersion and enhanced nonlinearity [1, 2]. The generation of narrowband frequency components in PCFs has attracted great attention. The compact ultrashort pulse sources, particularly in the visible and ultraviolet (UV) region of the electromagnetic spectrum, can find extensive applications in basic physical science. At present, studies are being carried out on supercontinuum [3–6] or non-supercontinuum [7–10] UV–visible sources based on the nonlinear effects in PCFs in order to up-convert the infrared pump energy into the visible and UV spectral band while retaining the requisite spectral and temporal characteristics. Although the selective spectral filtering of the supercontinuum can produce a multi-wavelength short pulse source, efforts to increase the blue-shift and extend the blue edge of the supercontinuum towards the UV region are difficult due to the complexity of generation; also, the temporal width can be elongated and the pulse energy decreased. The non-supercontinuum sources based on specific frequency conversion techniques such as four-wave mixing (FWM) [11–17], harmonics [18, 19], and dispersive waves (DWs) [20–23] are attractive because they minimize the loss of the pump pulse energy. The FWM and multi-frequency third-harmonics have generated tunable UV–visible signals in the fundamental guided mode but with a small average power or in an undesired higher-order mode. Moreover, the strong dependence on the phase-matching condition and the pulse walk-off effect have great limit on the conversion efficiency of the pump to signal. The DWs originating from the soliton self-frequency shift (SSFS) have been studied for generating the high power fundamental guided mode signals, but the experimental results only show the DWs at the visible wavelength in the solid-core PCFs. Recently, the ultrafast nonlinear optics in gas-filled hollow-core PCFs (HC-PCFs) have greatly progressed [24]. The emission of DWs in the deep-UV region is achieved in an Ar-filled HC-PCF, but the complex nonlinear optical properties of Ar and the effect of Ar-pressure on the dispersion of HC-PCF needs to be considered [25].

In this letter, for the first time to our knowledge, the broadband deep-UV to visible wavelengths are efficiently generated by the cross phase modulation (XPM) between the red-shifted solitons and the blue-shifted DWs in the fundamental guided mode of the multi-knots in a HC-PCF cladding (HC-PCFC). The multi-milliwatt ultrashort pulses can be tunable over the deep-UV (below 200 nm) to visible spectral region by adjusting the wavelengths of pump pulses coupled into different knots.

2. Knot properties and experiment

Figure 1(a) shows the cross-section of the HC-PCF fabricated in our laboratory. The complexing method of rectification and adsorption is used for purifying the silica material prepared by the plasma chemical vapor deposition (PCVD) to greatly reduce the intrinsic absorption losses of PCF at the UV (below 400 nm) and mid-infrared (above 2000 nm) wavelengths [26]. The average size of each knot in the cladding region is 1.38 μm. The pump pulses are coupled into the knots 1–3 marked in figure 1(a), and each knot can be viewed as a small solid-core feature where the nonlinear process of short pulse can be enhanced. The polarization of each knot is optimized, and the nonlinear energy transfer only takes place for the optimal polarization along the axes 1–3, as presented in the inset of figure 1(b). The calculated group velocity dispersion and the effective mode area for the fundamental guided mode

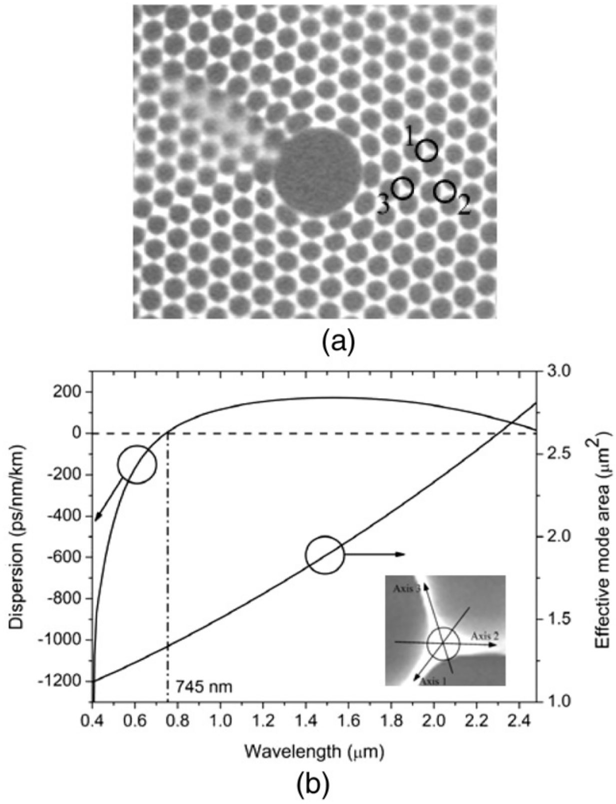

Figure 1. (a) The cross-section of HC-PCF used in the experiment, 1–3 represent the considered knots. (b) Group velocity dispersion and effective mode area calculated for the fundamental guided mode polarizing along axis 1 of knot 1 shown in the inset (the dispersion characteristics along axes 1–3 being very similar); the circled part denotes the size of knot 1, the vertical dashed line corresponds to the zero-dispersion wavelength of 745 nm.

polarized along axis 1 of knot 1 are presented in figure 1(b), where the first zero-dispersion wavelength is at 745 nm and the second one above 2500 nm is beyond consideration. The value of the effective mode area increases from 1.37 to 2.73 μm^2 as the radiation wavelength increases from 0.79 to 2.4 μm.

A mode-locked Ti:sapphire ultrafast laser, which emits a pulse train with FWHM of 120 fs and repetition rate of 76 MHz at the central wavelength of 800 nm, is used as the pump source. The near transformed limited pulses are obtained by compensating the group velocity dispersion with a pair of fused silica prisms. By the offset pumping technique, the fundamental mode can be selectively excited. The fiber length is optimized so that the solitons at the mid-infrared wavelengths and the spectral components at the UV wavelengths can keep a high level. An achromatic half-wave plate is used for aligning the polarization of the pump pulse to ensure a linearly polarized output. The optical beam is coupled into the knots of HC-PCFC which has a length of 50 cm. The coupling efficiency is 30%. Two optical spectrum analyzers (OSA, Avaspec-256 and Avaspec-NIR-256) with the measurement scopes of 200–1100 and 900–2500 nm and the wavelength resolutions of 0.025 and 15 nm are used to monitor the output spectra.

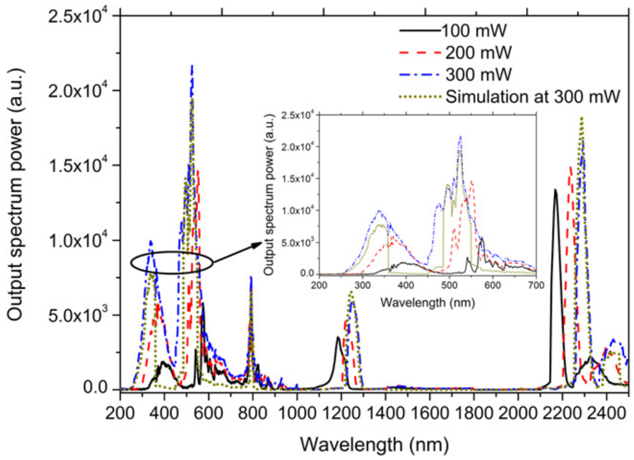

Figure 2. Output spectra at knot 1 for a pump wavelength of 790 nm and average powers of 100–300 mW. The short-dotted line corresponds to the simulation result using the NLSE at 300 mW. The inset shows the enlarged output spectra of the DW and UV spectral components.

3. Results and discussion

The femtosecond pulses are firstly coupled into knot 1. Taking into account the full complexity of the fiber group velocity dispersion, the self-phase modulation (SPM), XPM, the Raman contributions to the nonlinearity, the self-steeping (SS), and the loss of pump field, along with the nonlinear polarization term to include the influence of the wavelength-dependent effective mode area, the evolution of the pulse inside knot 1 can be described by solving the nonlinear Schrödinger equation (NLSE) [27, 28]. In the simulation, the parameters are chosen as follows: the pump peak power $P_p = 36$ kW, the FWHM of pulse $T_{FWHM} = 120$ fs, the nonlinear-index coefficient of fused silica $n_2 = 2.6 \times 10^{-20}$ m^2 W^{-1}, the second–sixth-order dispersion coefficient $\beta_2 = -2.0839$ and -3.4732 ps^2 km^{-1}, $\beta_3 = 0.549 \times 10^{-2}$ and 0.915×10^{-2} ps^3 km^{-1}, $\beta_4 = -1.4254 \times 10^{-6}$ and -2.3756×10^{-6} ps^4 km^{-1}, $\beta_5 = 1.2829 \times 10^{-8}$ and 2.0526×10^{-8} ps^5 km^{-1}, and $\beta_6 = -2.694 \times 10^{-10}$ and -4.3104×10^{-10} ps^6 km^{-1} at pump wavelengths of 790 and 850 nm, the fractional contribution of the Raman response $f_R = 0.18$, the characteristic times of the Raman response $\tau_1 = 12.5$ fs, and $\tau_2 = 32$ fs. The PCF length is 50 cm, the frequency-dependent nonlinear coefficient $\gamma(\omega)$ depends on the effective mode area, and the loss factor $\alpha(\lambda) = A\exp(-\alpha/\lambda)$. The simulation results with pump wavelengths of 790 and 850 nm at an average power of 300 mW agree well with the experimental ones, as presented in figures 2 and 3(a).

As shown in figure 2, when the pump wavelength is 790 nm and the average power is in the range of 100–300 mW, the fundamental solitons are formed in the

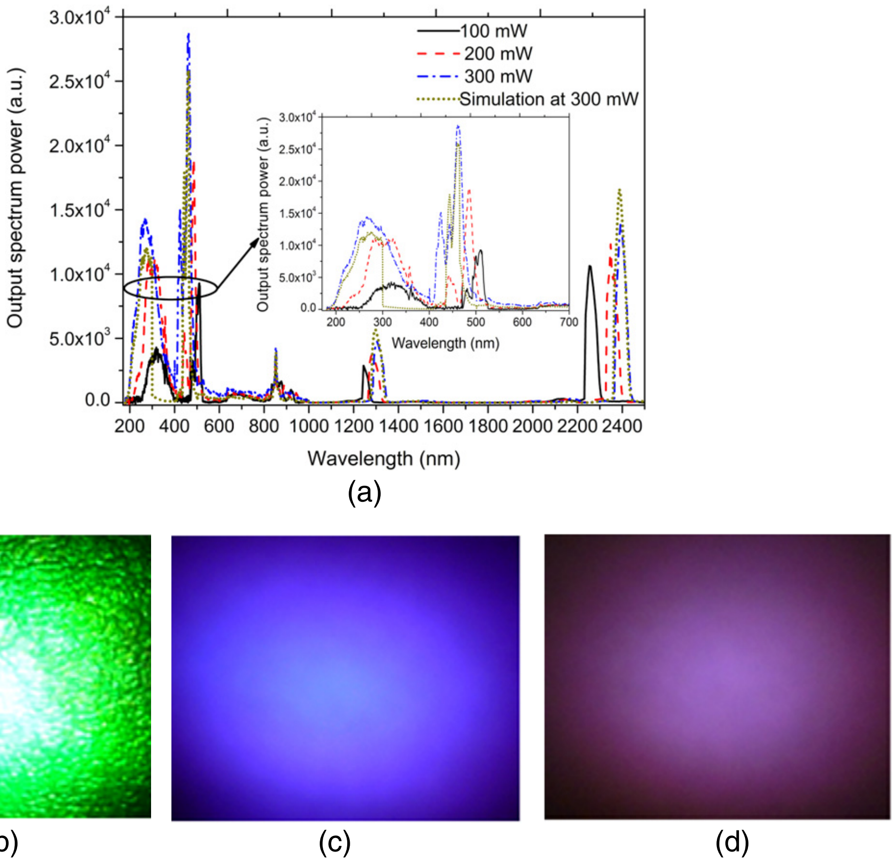

Figure 3. (a) Output spectra at knot 1 for a pump wavelength of 850 nm and average powers of 100–300 mW. The short-dotted line corresponds to the simulation result using the NLSE at 300 mW. The inset shows the enlarged output spectra of the DW and UV spectral components. (b)–(d) The observed output far fields of DWs with the green-blue, blue-violet, and violet light.

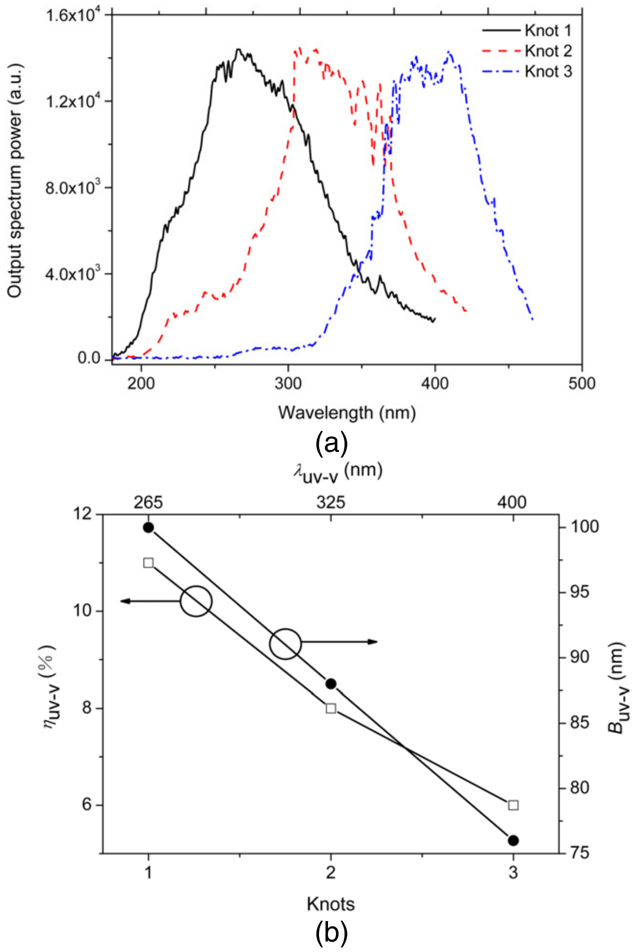

Figure 4. (a) Output spectra of the UV to visible spectral component at knots 1–3 for a pump wavelength of 850 nm and average power of 300 mW; (b) η_{uv-v} and B_{uv-v} of the UV to visible spectral component at different knots as a function of λ_{uv-v}.

anomalous dispersion region due to the interplay between the negative dispersion and SPM. As a result of the intrapulse Raman scattering (IRS), the first solitons gradually shift from 2168 to 2290 nm. The second solitons in the wavelength range of 1185–1250 nm generated from the residual pump are beyond consideration. Because of the perturbation induced by the higher-order dispersions and the resonance matching condition, the first solitons generate the DWs in the normal dispersion region at the short wavelength side of 575–525 nm, as shown in the inset. At the initial stage, the DWs have a slower group velocity than the solitons. However, as the soliton group velocities continuously decrease during the red-shift process, they will eventually meet with the DWs. Since the DWs are located on the trailing edges of the solitons, the temporal overlaps between the high power solitons and the DWs lead to the XPM, which generates spectral components at the shorter and longer wavelength sides than the DWs and solitons. As seen from figure 2 and the inset, the UV and mid-infrared spectral components of 400–335 and 2325–2440 nm are observed. The XPM process depends on the red-shift ability of the solitons, which can be limited by the material absorption loss above 2000 nm.

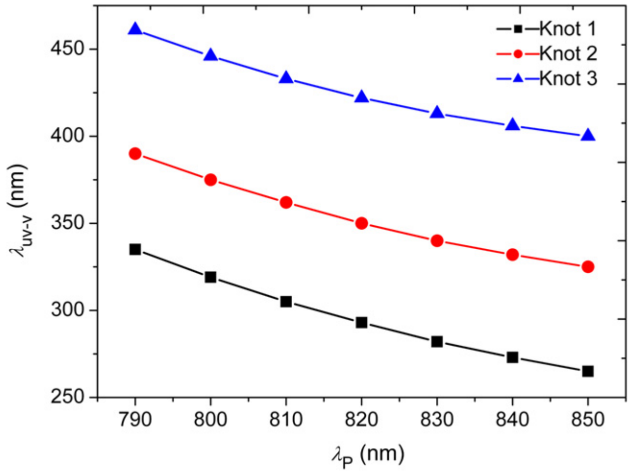

Figure 5. The changing relationship between λ_{uv-v} and λ_p with an average power of 300 mW at different knots.

When the average power of the pump pulse at 850 nm increases from 100–300 mW, the first solitons shift from 2256 to 2392 nm as the pump energies are greatly depleted, and the DW and UV spectral components are efficiently generated in the ranges of 508–462 and 325–265 nm, as shown in figure 3(a) and the inset. The SPM and normal dispersion experienced by the femtosecond pulses broaden the DW and UV spectra. The mid-infrared spectral components at the longer wavelength side than the solitons are not observed, and the main reasons considered are that they are completely depleted or generated beyond the measurement scope of OSA (above 2500 nm). In the SSFS process, except for the material absorption loss, the profiles of the group velocity dispersion and effective mode area, as shown in figure 1(b), also play important roles. The red-shift of the soliton can be halted by the spectral recoil as the soliton approaches the second zero-dispersion wavelength and the balance between the diffraction and index-step guiding in the knot is broken due to the increase of effective mode area. Although the knot also supports the higher-order modes in the UV region, the poor modal overlap with the pump light and the absence of phase matching to resonant radiation mean that they are not excited. The observed output far fields of DWs are shown in figures 3(b)–(d), where the field intensities are maximal at the center of the knot core and monotonically decrease with the distance from the core center, showing the distribution characteristics of a fundamental guided mode.

When the pump operates at 850 nm with an average power of 300 mW in knots 1–3, the central wavelengths of the generated UV to visible spectral component λ_{uv-v} are 265, 325, and 400 nm, as shown in figure 4(a). The conversion efficiency η_{uv-v} is defined as the ratio of the UV–visible power P_{uv-v} to the total transmitted power in the knots P_t. For a coupling efficiency of 30%, P_{uv-v} are measured to be 9.9, 7.2, and 5.4 mW, η_{uv-v} can be up to 11%, 8%, and 6%, and the bandwidths B_{uv-v} are 100, 88, and 76 nm, as shown in figure 4(b). For knot 1, the spectral component with η_{uv-v} of 11% and B_{uv-v} of 100 nm in the deep-UV region is obtained.

As presented in figure 5, when the pump pulses with average power of 300 mW are coupled into knots 1–3 and the pump wavelength λ_p is adjusted from 790 to 850 nm with an interval of 10 nm, λ_{uv-v} changes from 335 to 265 nm, 390 to 325 nm, and 461 to 400 nm, and the wavelength-tunable range can be about 200 nm (265 to 461 nm). Because of the special dispersion characteristics of different knots, it can be expected that the central wavelengths of ultrashort pulses generated by the XPM can be tunable over the deep-UV (below 200 nm) to visible region by coupling the femtosecond pulses into other knots. Because of the normal dispersion and SPM, the widths of short pulses generated at 265, 325, and 400 nm are measured to be 30, 37, and 46 fs by the Talbot effect.

4. Conclusion

In summary, the deep-UV to visible wavelengths by XPM in the fundamental guided mode of the multi-knots of a HC-PCFC are experimentally generated. The high conversion efficiency, broad bandwidth, and widely tunable deep-UV to visible spectra can constitute an important progress in the development of a simple and compact ultrashort deep-UV to visible pulse source. It can find important applications in ultrafast photonics, femtochemisty, photobiology, and UV–visible resonant Raman scattering.

Acknowledgments

This work is partly supported by the National Basic Research Program (2010CB327605 and 2010CB328300), the National High-Technology Research and Development Program of China (2013AA031501), the key grant of the Ministry of Education (109015), the Program for New Century Excellent Talents in University (NECT-11-0596), the Beijing Nova program (2011066), the Specialized Research Fund for the Doctoral Program of Higher Education (20120005120021), the Fundamental Research Funds for the Central Universities (2013RC1202), the China Postdoctoral Science Foundation (2012M511826), the Postdoctoral Science Foundation of Guangdong Province (244331), the Open Fund of the State Key Laboratory of Information Photonics and Optical Communications (Beijing University of Posts and Telecommunications) P R China, and the Science Foundation Ireland (07/SK/I1200 and 07/SK/I1200-ISTTF11).

References

[1] Russell P St J 2006 *J. Lightwave Technol.* **24** 4729–49
[2] Dudley J M and Taylor J R 2009 *Nature Photon.* **3** 85–90
[3] Dudley J M, Genty G and Coen S 2005 *Rev. Mod. Phys.* **78** 1135–84
[4] Kudlinski A, George A K, Knight J C, Travers J C, Rulkov A B, Popov S V and Taylor J R 2006 *Opt. Express* **14** 5715–22
[5] Lin J H, Lin K H, Hsu C C, Yang W H and Hsieh W F 2007 *Laser Phys. Lett.* **4** 413–7
[6] Frosz M H, Moselund P M, Rasmussen P D, Thomsen C L and Bang O 2008 *Opt. Express* **16** 21076–86
[7] Tu H H and Boppart S A 2009 *Opt. Express* **17** 17983–8
[8] Hu M L, Wang C Y, Chai L, Li Y F, Dukel'skii K V, Khokhlov A V, Shevandin V S, Kondrat'ev Yu N and Zheltikov A M 2004 *Laser Phys. Lett.* **1** 299–302
[9] Fedotov A B, Serebryannikov E E, Ivanov A A, Mel'nikov L A, Shcherbakov A V, Sidorov-Biryukov D A, Sun Ch-K, Alfimov M V and Zheltikov A M 2006 *Laser Phys. Lett.* **3** 301–5
[10] Mitrokhin V P, Ivanov A A, Fedotov A B, Alfimov M V, Dukel'skii K V, Khokhlov A V, Shevandin V S, Kondrat'ev Yu N, Podshivalov A A and Zheltikov A M 2007 *Laser Phys. Lett.* **4** 529–33
[11] Abedin K S, Gopinath J T, Ippen E P, Kerbage C E, Windeler R S and Eggleton B J 2002 *Appl. Phys. Lett.* **81** 1384–6
[12] Husakou A V and Herrmann J 2003 *Appl. Phys. Lett.* **83** 3867–9
[13] Akimov D A, Serebryannikov E E, Zheltikov A M, Schmitt M, Maksimenka R, Kiefer W, Dukel'skii K V, Shevandin V S and Kondrat'ev Yu N 2003 *Opt. Lett.* **28** 1948–50
[14] Konorov S O *et al* 2004 *Laser Phys. Lett.* **1** 402–5
[15] Tu H, Jiang Z, Marks D L and Boppart S A 2009 *Appl. Phys. Lett.* **94** 101109
[16] Yuan J H, Sang X Z, Yu C X, Li S G, Zhou G Y and Hou L T 2010 *IEEE J. Quantum Electron.* **46** 728–33
[17] Yuan J H, Sang X Z, Yu C X, Han Y, Zhou G Y, Li S G and Hou L T 2011 *J. Lightwave Technol.* **29** 2920–6
[18] Ivanov A A, Lorenc D, Bugar I, Uherek F, Serebryannikov E E, Konorov S O, Alfimov M V, Chorvat D and Zheltikov A M 2006 *Phys. Rev.* E **73** 016610
[19] Fedotov A B, Voronin A A, Serebryannikov E E, Fedotov I V, Mitrofanov A V, Ivanov A A, Sidorov-Biryukov D A and Zheltikov A M 2007 *Phys. Rev.* E **75** 016614
[20] Cristiani I, Tediosi R, Tartara L and Degiorgio V 2004 *Opt. Express* **12** 124–35
[21] Chang G Q, Chen L J and Kärtner F X 2010 *Opt. Lett.* **35** 2361–3
[22] Yuan J H, Sang X Z, Yu C X, Han Y, Zhou G Y, Li S G and Hou L T 2011 *IEEE Photon. Technol. Lett.* **23** 786–8
[23] Yuan J H *et al* 2013 *Laser Phys. Lett.* **10** 045405
[24] Travers J C, Chang W, Nold J, Joly N Y and Russell P St J 2011 *J. Opt. Soc. Am.* B **28** A11–26
[25] Joly N Y, Nold J, Chang W, Hölzer P, Nazarkin A, Wong G K L, Biancalana F and Russell P St J 2011 *Phys. Rev. Lett.* **106** 203901
[26] Hu X Z, Zou L S and Liu Y X 1998 *Fiber Optic Cable and Engineering Application* (Beijing: Academic)
[27] Serebryannikov E E, Zheltikov A M, Köhler S, Ishii N, Teisset C Y, Fuji T, Krausz F and Baltuška A 2006 *Phys. Rev.* E **73** 066617
[28] Peng J H, Sokolov A V, Benabid F, Biancalana F, Light P S, Couny F and Roberts P J 2010 *Phys. Rev.* A **81** 031803(R)